24 Ringden O, Uzunel M, Rasmusson I *et al.* Mesenchymal stem cells for treatment of therapy-resistant graft-versus-host disease. *Transplantation* 2006; **81**: 1390–7.
25 Bunnell BA, Deng W, Robinson CM *et al.* Potential application for mesenchymal stem cells in the treatment of cardiovascular diseases. *Can. J. Physiol. Pharmacol.* 2005; **83**: 529–39.
26 El-Badri NS, Maheshwari A, Sanberg PR. Mesenchymal stem cells in autoimmune disease. *Stem Cells Dev.* 2004; **13**: 463–72.
27 Maestroni GJ, Hertens E, Galli P. Factor(s) from nonmacrophage bone marrow stromal cells inhibit Lewis lung carcinoma and B16 melanoma growth in mice. *Cell. Mol. Life Sci.* 1999; **55**: 663–7.
28 Ohlsson LB, Varas L, Kjellman C *et al.* Mesenchymal progenitor cell-mediated inhibition of tumor growth *in vivo* and *in vitro* in gelatin matrix. *Exp. Mol. Pathol.* 2003; **75**: 248–55.
29 Pisati F, Belicchi M, Acerbi F *et al.* Effect of human skin-derived stem cells on vessel architecture, tumor growth, and tumor invasion in brain tumor animal models. *Cancer Res.* 2007; **67**: 3054–63.
30 Zhu W, Xu W, Jiang R *et al.* Mesenchymal stem cells derived from bone marrow favor tumor cell growth *in vivo*. *Exp. Mol. Pathol.* 2006; **80**: 267–74.
31 Sasser AK, Sullivan NJ, Studebaker AW *et al.* Interleukin-6 is a potent growth factor for ER-alpha-positive human breast cancer. *FASEB J.* 2007; **21**: 3763–70.
32 Kucerova L, Altanerova V, Matuskova M *et al.* Adipose tissue-derived human mesenchymal stem cells mediated prodrug cancer gene therapy. *Cancer Res.* 2007; **67**: 6304–13.
33 Vesselinovitch SD, Mihailovich N. Kinetics of diethylnitrosamine hepatocarcinogenesis in the infant mouse. *Cancer Res.* 1983; **43**: 4253–9.
34 Peng L, Xie DY, Lin BL *et al.* Autologous bone marrow mesenchymal stem cell transplantation in liver failure patients caused by hepatitis B: short-term and long-term outcomes. *Hepatology* 2011; **54**(3): 820–8.
35 Koen H, Pugh TD, Nychka D *et al.* Presence of alpha-fetoprotein-positive cells in hepatocellular foci and microcarcinomas induced by single injections of diethylnitrosamine in infant mice. *Cancer Res.* 1983; **43**: 702–8.
36 Yoshida H, Shiratori Y, Moriyama M *et al.* Interferon therapy reduces the risk for hepatocellular carcinoma: national surveillance program of cirrhotic and noncirrhotic patients with chronic hepatitis C in Japan. IHIT Study Group. Inhibition of hepatocarcinogenesis by interferon therapy. *Ann. Intern. Med.* 1999; **131**: 174–81.
37 Sakaida I, Hironaka K, Uchida K *et al.* Fibrosis accelerates the development of enzyme-altered lesions in the rat liver. *Hepatology* 1998; **28**: 1247–52.
38 Terai S, Yamamoto N, Omori K *et al.* A new cell therapy using bone marrow cells to repair damaged liver. *J. Gastroenterol.* 2002; **37** (Suppl. 14): 162–3.
39 Alwayn IP, Verbesey JE, Kim S *et al.* A critical role for matrix metalloproteinases in liver regeneration. *J. Surg. Res.* 2008; **145**: 192–8.
40 Higashiyama R, Inagaki Y, Hong YY *et al.* Bone marrow-derived cells express matrix metalloproteinases and contribute to regression of liver fibrosis in mice. *Hepatology* 2007; **45**: 213–22.
41 Moriya K, Nakagawa K, Santa T *et al.* Oxidative stress in the absence of inflammation in a mouse model for hepatitis C virus-associated hepatocarcinogenesis. *Cancer Res.* 2001; **61**: 4365–70.
42 Kemp K, Hares K, Mallam E *et al.* Mesenchymal stem cell-secreted superoxide dismutase promotes cerebellar neuronal survival. *J. Neurochem.* 2010; **114**: 1569–80.
43 Kemp K, Gordon D, Wraith DC *et al.* Fusion between human mesenchymal stem cells and rodent cerebellar Purkinje cells. *Neuropathol. Appl. Neurobiol.* 2011; **37**: 166–78.

Cell Tissue Res (2011) 346:79–88
DOI 10.1007/s00441-011-1236-0

REGULAR ARTICLE

TNFR1-mediated signaling is important to induce the improvement of liver fibrosis by bone marrow cell infusion

Takuro Hisanaga · Shuji Terai · Takuya Iwamoto · Taro Takami · Naoki Yamamoto · Tomoaki Murata · Toshifumi Matsuyama · Hiroshi Nishina · Isao Sakaida

Received: 25 April 2011 / Accepted: 30 August 2011 / Published online: 11 October 2011

Abstract The importance of TNF-α signals mediated by tumor necrosis factor receptor type 1 (TNFR1) in inflammation and fibrosis induced by carbon tetrachloride (CCl_4), and in post-injury liver regeneration including a GFP/CCl_4 model developed as a liver repair model by bone marrow cell (BMC) infusion, was investigated. In mice in which TNFR1 was suppressed by antagonist administration or by knockout, liver fibrosis induced by CCl_4 was significantly decreased. In these mice, intrahepatic macrophage infiltration and TGF-β1 expression were reduced and stellate cell activity was decreased; however, expression of MMP-9 was also decreased. With GFP-positive BMC (TNFR1 wild-type, WT) infusion in these mice, fibrosis proliferation, including host endogenous intrahepatic macrophage infiltration, TGF-β1 expression and stellate cell activity, increased significantly. There was no significant increase of MMP-9 expression. In this study, TNFR1 in hosts had a promoting effect on CCl_4-induced hepatotoxicity and fibrosis, whereas BMC infusion in TNFR1 knockout mice enhanced host-derived intrahepatic inflammation and fibrosis proliferation. These findings differed from those in WT recipient mice, in which improvement in inflammation and fibrosis with BMC infusion had previously been reported. TNFR1-mediated signaling might be important to induce the improvement of liver fibrosis by bone marrow cell infusion.

Keywords Tumor necrosis factor · CCl_4 · Bone marrow cell · Liver cirrhosis · Hepatic stellate cell

T. Hisanaga · S. Terai (✉) · T. Iwamoto · T. Takami · N. Yamamoto · I. Sakaida
Department of Gastroenterology & Hepatology,
Yamaguchi University Graduate School of Medicine,
Minami Kogushi 1-1-1,
Ube, Yamaguchi 755-8505, Japan
e-mail: terais@yamaguchi-u.ac.jp

T. Murata
Institute of Laboratory Animals, Yamaguchi University,
Minami Kogushi 1-1-1,
Ube, Yamaguchi 755-8505, Japan

T. Matsuyama
Department of Molecular Microbiology and Immunology,
Nagasaki University Graduate School of Biomedical Sciences,
1-12-4 Sakamoto,
Nagasaki 852-8523, Japan

H. Nishina
Department of Developmental and Regenerative Biology,
Medical Research Institute, Tokyo Medical and Dental University,
Yushima 1-5-45,
Bunkyo-ku, Tokyo 113-0034, Japan

Introduction

The mechanism of hepatotoxicity induced by many factors, including CCl_4, has been studied for a long time (Drill 1952) and besides direct cytotoxicity due to these factors, enhanced hepatotoxicity due to inflammatory cell infiltration and stellate cell activation induced by these factors also occurs. TNF-α is an important inflammatory cytokine that induces hepatotoxicity; however, it also initiates liver regeneration after injury. This has been examined in various previous hepatotoxicity, hepatic resection and hepatic failure models. In addition, in recent stem cell studies, TNF-α signals have been found to be essential in the differentiation/proliferation process from stem cells to functional cells. For effective expression of TNF-α signals, of the various receptors, TNFR1 (p55) is important. In

studies using TNFR1 knockout (KO) mice, while inhibition of hepatotoxicity has been shown, decreased liver regeneration and hepatocyte proliferation have also been confirmed (Gardner et al. 2003; Simeonova et al. 2001; Sudo et al. 2005; Yamada and Fausto 1998).

In our laboratory, using a GFP/CCl_4 model, BMC infusion has been shown to improve fibrosis and liver function in cirrhosis (Sakaida et al. 2004, 2008; Terai et al. 2002, 2005). In the liver of mice not treated with CCl_4, without hepatic toxicity, repopulation of GFP-positive BMCs into the liver has not been observed, thus highlighting the need for chronic inflammatory signals in cell repopulation and effective expression. In addition, after BMC infusion, alterations in TNFR1 expression and associated increases in various cytokines such as fibroblast growth factor 2 (FGF2) have been recognized (Omori et al. 2004). This also suggested the importance of inflammatory signals, particularly TNF-α signals, in liver function improvement. Therefore, to investigate the importance of TNF-α signals mediated by TNFR1 in liver repair by BMC infusion in recipients, this study using TNFR1 antagonist-administered mice and TNFR1 KO mice as recipients was conducted.

Materials and methods

Mice

C57BL/6 TNFR1 KO mice were kindly provided by Hiroshi Nishina (Department of Developmental and Regenerative Biology, Medical Research Institute, Tokyo Medical and Dental University). TNFR1 KO mouse typing was performed by PCR analysis using primer typing box [p55R636 and HSV-TK (to confirm induction of silencing gene factor)]. Those primers were p55R636 (5′-GGCTGCAGTCCACGCACTGG-3′), and HSV-TK (5′-ATTCGCCAATGACAAGACGCTGG-3′) (data not shown) (Pfeffer et al. 1993). C57BL/6 female mice were purchased from Chiyoda SLC (Tokyo, Japan). GFP-transgenic mice (TgN(β-act-EGFP)Osb) were kindly provided by Masaru Okabe (Genome Research Center, Osaka University, Osaka, Japan). These mice were maintained in specific pathogen-free housing at the Animal Experiment Facility of Yamaguchi University School of Medicine and cared for in accordance with the animal ethics requirements at Yamaguchi University School of Medicine.

Experimental protocol

First, to confirm that signals mediated by TNFR1 are important in intrahepatic inflammatory responses and fibrosis induced by CCl_4, an experiment using TNFR1 antagonist (anti-mouse TNFR1 antibody, MAB430; R&D Systems, Minneapolis, MN, USA) was conducted in wild-type (WT) mice. In WT mice, CCl_4 was administered for 4 weeks to create a liver cirrhosis model; then, by caudal vein injection of 100 μg/body of antagonist, signals mediated by TNFR1 were suppressed in recipients; and thereafter, CCl_4 was continued for 1 week. A model was also created with infusion of GFP-positive BMCs after 1 h, when in vivo activity of the antagonist reaches a peak. There were 3 groups: WT (Control) (wild-type, without BMC infusion); WT+A (wild-type, with TNFR1 antagonist only, without BMC infusion); and GFP/WT+A (wild-type, with TNFR1 antagonist and with BMC infusion) (Fig. 1).

As will be described later, by blocking TNFR1, suppression of fibrosis and suppression of inflammatory cell infiltration were confirmed. Therefore, as a more highly specific model, a model was created by the following protocol with TNFR1 KO mice as BMC infusion recipients.

Six-week-old female C57BL/6 mice and female isogenic TNFR1 KO mice were treated with CCl_4 (1.0 ml/kg body diluted 1:3 in corn oil) twice a week for 8 weeks. In the other group, after 4 weeks of CCl_4 administration in each group (C57BL/6 wild-type and TNFR1 KO), bone marrow cells (BMC) (1×10^5 cells) from GFP transgenic mice were injected via the tail vein as previously described (Terai et al. 2003).

After 8 weeks, 36 h after the last CCl_4 injection, the mice were sacrificed to examine the blood data and liver tissue specimens. The liver was fixed in 4% buffered paraformaldehyde for 24–48 h and paraffin embedded. Blood samples were obtained by cardiac puncture and drawn into a glass tube containing 7.5% EDTA (pH 7.4). After centrifugal separation, the plasma was stored at 4°C.

There was a total of 4 groups in this study: WT (Control), wild-type without BMC infusion; KO (Control), TNFR1 KO without BMC infusion; GFP/WT, wild-type with GFP-positive BMC infusion; and GFP/KO, TNFR1 KO with GFP-positive BMC infusion (Fig. 1).

Quantitative analysis of liver fibrosis and immunohistochemistry

The liver fibrosis area was quantified with Sirius-red staining using an Olympus Provis microscope equipped with a CCD camera (Olympus, Tokyo, Japan). The red area, considered the fibrotic area, was assessed by computer-assisted image analysis with MetaMorph software (Universal Imaging, Downingtown, PA, USA) at a magnification of ×40. The mean value of 10 randomly selected areas per sample was used as the expressed percent area of fibrosis.

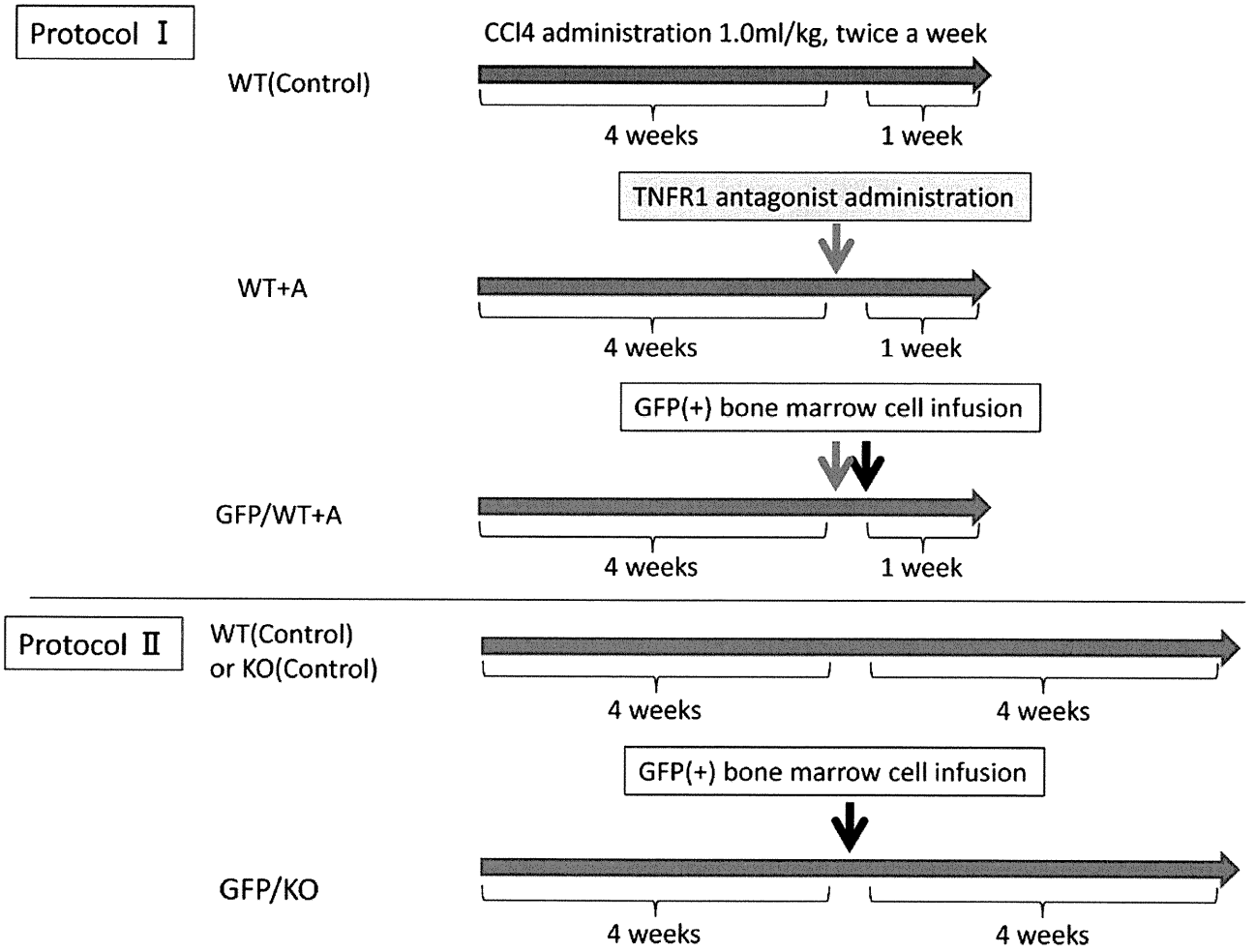

Fig. 1 Experimental protocols. *Protocol I* In each group of mice, CCl_4 (1.0 ml/kg body) was administered twice a week for 5 weeks to create a liver cirrhosis model. In WT+A mice, 100 μg/body of TNFR1 antagonist was injected via tail vein before 1 week of sacrifice. GFP/WT+A mice were treated with GFP positive BMC (1×10^5 cells) infusion via tail vein 1 hour after TNFR1 antagonist injection. *Protocol II* WT (Control) mice and KO (Control) mice were treated with CCl_4 (same as above) for 8 weeks. In GFP/WT mice and GFP/KO mice, after 4 weeks of CCl_4 administration, BMCs (1×10^5 cells) were injected, followed by 4 weeks of CCl_4 treatment

Immunohistochemistry of TGF-β1, alpha smooth muscle actin (α-SMA), matrix metalloproteinase (MMP)-9 and F4/80

Three-μm-thick liver sections were mounted on microscope slides, routinely dewaxed and rehydrated and pretreated with Vector Antigen Unmasking Solutions (Citrate-based, Cat. No. H-3300). For the immunohistochemical analysis, the Vectastain ABC kit (Vector Laboratories, Burlingame, CA, USA) was used for GFP (anti-GFP, rabbit IgG fraction, A11122; Invitrogen, Carlsbad, CA, USA), TGF-β1[TGF-β1(V), SC-146; Santa Cruz Biotechnology], alpha-smooth muscle actin (α-SMA) (alpha smooth muscle actin antibody, ab6594; Abcam, Cambridge, MA, USA), matrix metalloproteinase (MMP)-9 (anti-mouse MMP-9 antibody, AF909; R&D Systems) and F4/80 [F4/80 antibody(BM8), ab16911; Abcam] staining by the avidin-biotin-peroxidase complex method.

Additionally, double immunofluorescent staining was performed to study co-expression of GFP and F4/80 in bone marrow cell-infused mice. The mixture of the first antibodies was GFP and F4/80 noted above. The secondary antibodies, goat anti-rabbit IgG (H+L), Alexa Fluor 488 (A11034,;Invitrogen) (Green) and goat anti-rat IgG (H+L), Alexa Fluor 568 (A11077; Invitrogen) (Red) were each applied at a concentration of 1:400 in PBS for 60 min at room temperature. Before attaching the coverslip, DAPI (D212; Dojindo Laboratories, Kumamoto, Japan) was applied for counterstaining to visualize all nuclei in the tissue sections. The sections were viewed and photographed with the CCD camera noted above.

Real-time quantitative PCR analysis

Total RNA was isolated from the livers of the mice treated at 4 weeks after the BMC infusion or control CCl_4 treatment. The messenger RNA (mRNA) expressions of TGF-β1 and MMP-9 were evaluated using real-time quantitative PCR. Total RNA was extracted using the RNeasy Mini Kit (Qiagen, Hilden, Germany). For cDNA synthesis, AMV reverse transcription reagents were used according to the manufacturer's instructions (Roche Diagnostic, Pleasanton, CA, USA). Real-time PCR was performed with SYBR Green Master Mix (Roche Diagnostic). The primers used for TGF-β1 were 5′-GAAGCCATCCGTGGCCAGAT-3′ (forward) and 5′-GACGTCAAAAGACAGCACT-3′ (reverse), for MMP-9 were 5′-GGAACTCACACGACATCTTCCA-3′ (forward) and 5′-GAAACTCACACGCCAGAAGAATTT-3′ (reverse) and collagen type 1 alpha were 5′-CGGGCAG GACTTGGGTA-3′ (forward) and 5′-CGGAATCT GAATGGTCTGACT-3′ (reverse). The PCR primers used for mouse glyceraldehyde-3-phospatase dehydrogenase (GAPDH), which was used as an internal control, were: 5′-GTCTTCACCACCATGGAGAAGGC-3′, 5′-ATG CCAGTGAGCTTCCCGTTCAGC-3′. The cycle for PCR was as follows: 1 cycle of 95°C for 20 s; 40 cycles of 3 s at 95°C and 30 s at 60°C; and 1 cycle of 95°C for 15 s, 60°C for 1 min, and 95°C for 15 s. Reactions were performed in a Step One Plus™ real-time PCR system (Applied Biosystems, California, CA, USA) and amounts of all mRNAs were quantified using StepOne™ version 2.1 software (Applied Biosystems).

Western blot analysis

The liver samples (approximately 40 mg) were homogenized in 1 ml of cell lysis buffer (Cell Signal Technology, Beverly, MA, USA) and 1 mM phenylmethanesulfonyl fluoride (PMSF) and complete mini-centrifuged (Roche Diagnostic). The supernatant represented the whole protein. Then, 40 μg of the protein sample were mixed with the same volume of loading buffer (5% 2-mercaptoethanol and 95% Laemmli Sample Buffer; Bio-Rad Laboratories, Hercules, CA, USA), heated for 4 min at 97°C and separated by 10% SDS-PAGE. The separated bands were transferred to Immobilon-P transfer membrane (Millipore, Billerica, MA, USA), followed by blocking of the membranes for 1 h with blocking buffer (0.1% Tween-20; Wako Pure Chemical Industries, Osaka, Japan), 0.2% I-Block™ reagent (Tropix, Bedford, MA, USA) and 1 mM Tris-HCl buffer (pH 7.5) (Invitrogen). The membranes were then washed with washing buffer (0.1% Tween-20, 1 mM Tris-HCl buffer; pH 7.5) and incubated overnight at 4°C with the primary antibodies against MMP-9 (R&D Sytems), TGF-β1 (Santa Cruz Biotechnology) and β-actin (Abcam) in blocking buffer. Then, after being washed, the membranes were incubated for 1 h at room temperature with the appropriate secondary antibodies. Reactive bands were identified using ECL (Amersham Biosciences, Piscataway, NJ, USA) and autoradiography, according to the manufacturer's instructions.

Statistical analysis

Statistical significance was determined using 2-tailed Student's *t* test. Results are presented as the mean±standard deviation and differences of $p<0.05$ were considered significant.

Results

Alterations of liver fibrosis and intrahepatic inflammatory invasion by TNFR1 antagonist and BMC infusion

At 1 week after TNFR1 antagonist administration in wild-type mice, liver fibrosis was significantly suppressed [WT (Control): WT+A, $p<0.01$] in the antagonist-treated group compared to the untreated group. In addition, F4/80-positive intrahepatic macrophage infiltration tended to be suppressed [WT (Control): WT+A, $p=0.07$] and stellate cell activity, shown by α-SMA staining, was significantly suppressed [WT (Control): WT+A, $p<0.01$]. However, in the group with GFP-positive BMC infusion in addition to the antagonist, liver fibrosis did not improve with BMC infusion (WT+A: GFP/WT+A, $p=0.44$) Conversely, both macrophage infiltration (WT+A: GFP/WT+A, $p=0.02$) and stellate cell activity (WT+A: GFP/WT+A, $p<0.01$) increased significantly (Fig. 2a–l).

Liver fibrosis did not improve in the KO recipient model

The migration of GFP positive cells was confirmed using immunohistochemistry of GFP (Fig. 3a, b). On Sirius red staining, liver fibrosis was significantly suppressed in KO (Control) mice compared to WT (Control) mice [WT (Control): KO (Control), $p<0.05$]. WT mice tended to have strong fibrosis but similar to the GFP/CCl_4 model that we previously reported (Terai, et al. 2003), with BMC infusion, fibrosis improved significantly [WT (Control): GFP/WT, $p<0.01$]. However, in TNFR1 KO mice, in whom fibrosis was suppressed, BMC infusion did not improve liver fibrosis [KO (Control): GFP/KO, $p = 0.91$] (Fig. 3c–g).

In addition, on real-time RT-PCR for collagen I-α1, in WT mice, fibrosis proliferation was increased and in KO mice, it was suppressed [WT (Control): KO (Control), $p< 0.05$]. In WT mice, as in our previous GFP/CCl_4 model,

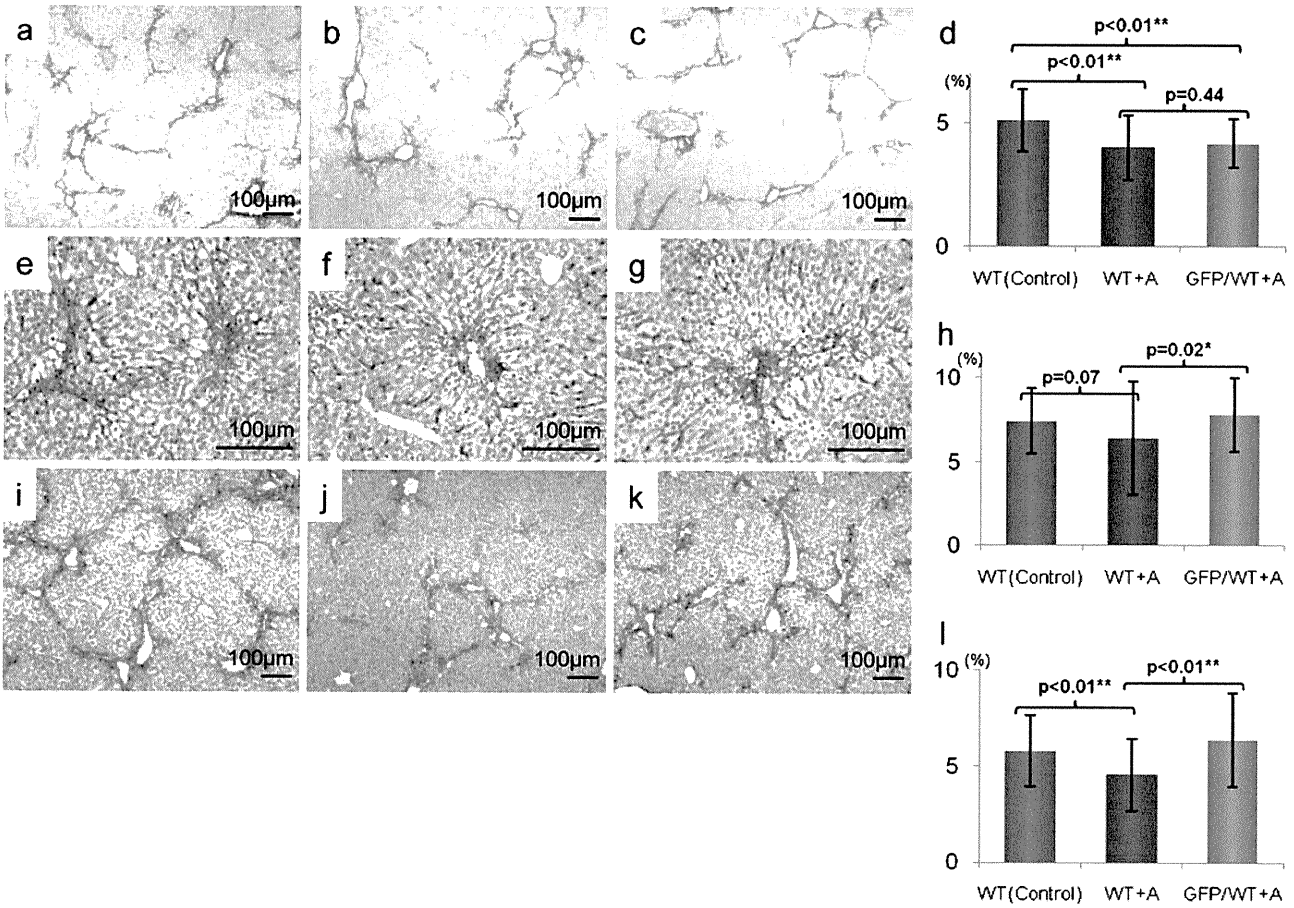

Fig. 2 Suppression of liver fibrosis, hepatic stellate cell activation and F4/80 positive cell invasion using TNFR1 antagonist. **a–c** Sirius red staining of liver sections (original magnifications ×40). **d** Statistical analysis of fibrotic area by the staining. *Scale bars* standard deviations. WT liver (**a**) had severe fibrosis but WT+A liver (**b**) and GFP/WT+A liver (**c**) did not. There was no significant improvement induced by BMC infusion with TNFR1 antagonist. **e–g** Immunohistochemistry of F4/80 (original magnifications ×100). **h** Statistical analysis of F4/80 positive area. Comparing WT (**e**) with WT+A (**f**), TNFR1 antagonist suppressed the invasion of F4/80 positive cells into the liver but in GFP/WT+A (**g**), the invasion increased. **i–k** Immunohistochemistry of α-SMA (original magnifications ×40). **l** Statistical analysis of α-SMA positive area. Comparing WT (**i**) with WT+A (**j**), TNFR1 antagonist suppressed the expression of α-SMA but in GFP/WT+A (**k**), the bone marrow cell infusion raised the activation regardless of TNFR1 antagonist administration

after BMC infusion, collagen I-α1 mRNA expression was decreased [WT (Control): GFP/WT, $p<0.05$]. On the other hand, there were no changes in KO mice with BMC infusion [KO (Control): GFP/KO, $p=0.67$] (Fig. 3h).

Fibrolytic reactions induced by BMC infusion

Expression of MMP-9, important in liver fibrosis improvement, corresponded with sites of inflammation and fibrosis in each model and based on western blot and real-time RT-PCR analysis, MMP-9 expression was significantly suppressed in KO mice compared to wild-type mice [WT (Control): KO(Control), $p<0.01$]. However, in KO mice, even with GFP-positive BMC infusion, there was no significant increase, statistically proven in Real-time RT-PCR analysis [KO (Control): GFP/KO, $p=0.41$]. This showed that, in KO mice, although MMP-9 expression is suppressed, BMC infusion in these mice did not clearly increase MMP-9 (Fig. 3i-n).

Alterations of F4/80 positive cells into TNFR1 KO mice

In KO (Control) mice, compared to WT (Control) mice, intrahepatic infiltration of F4/80-positive cells (macrophages) induced by CCl_4 was significantly suppressed [WT (Control): KO (Control), $p<0.01$] but with BMC infusion, this infiltration was significantly increased [KO (Control): GFP/KO, $p<0.01$] (Fig. 4a–e). Upon evaluation of macrophage origin, in double immunofluorescent staining (GFP: emitting green light, and F4/80: emitting red light), no cells showed co-positivity with GFP and F4/80. It was indicated that the increased F4/80-positive macro-

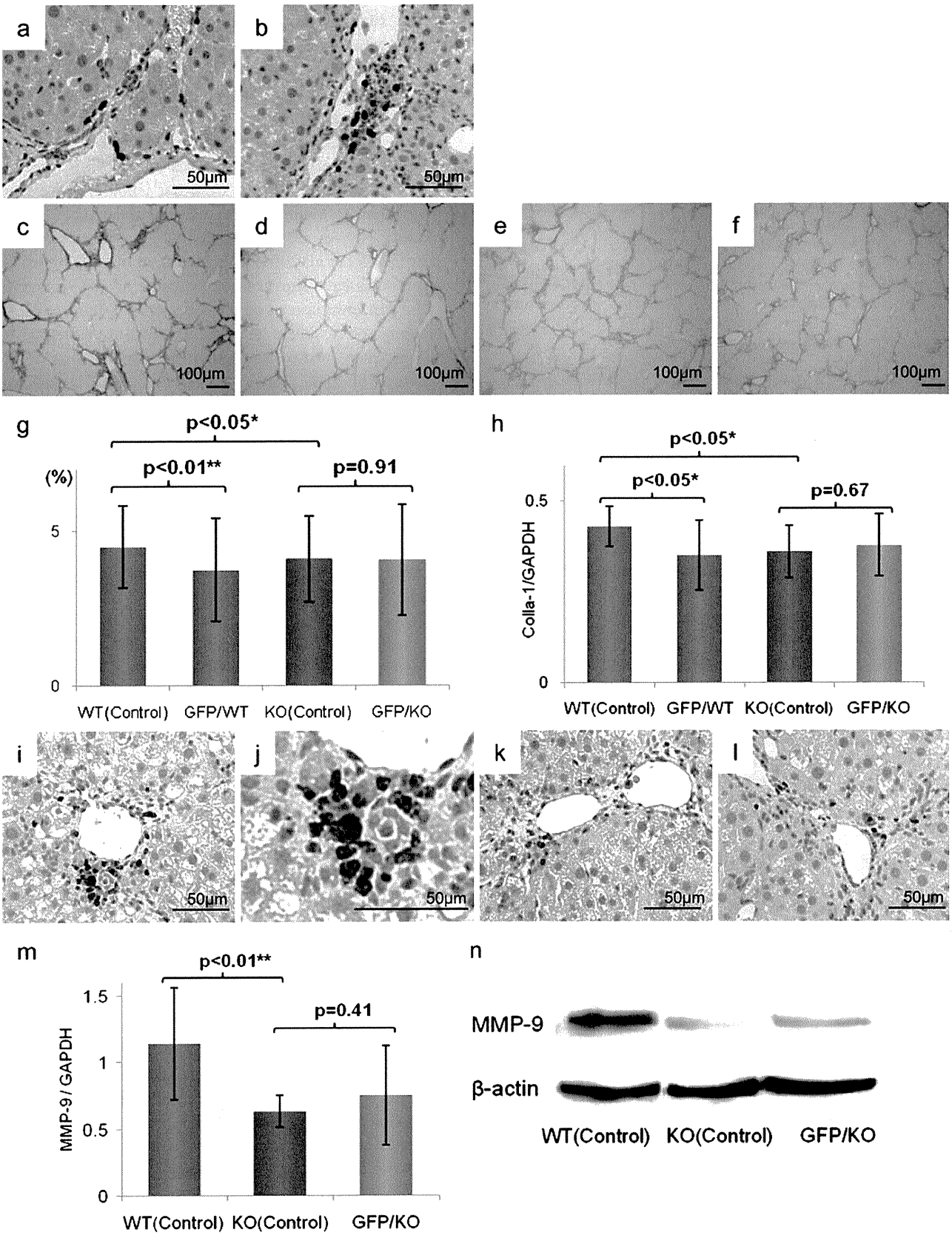
a
b
50μm
50μm
c
d
e
f
100μm
100μm
100μm
100μm
g
p<0.05*
p<0.01**
p=0.91
(%)
5
0
WT(Control)
GFP/WT
KO(Control)
GFP/KO
h
p<0.05*
p<0.05*
p=0.67
0.5
0
Colla-1/GAPDH
WT(Control)
GFP/WT
KO(Control)
GFP/KO
i
j
k
l
50μm
50μm
50μm
50μm
m
p<0.01**
p=0.41
1.5
1
0.5
0
MMP-9 / GAPDH
WT(Control)
KO(Control)
GFP/KO
n
MMP-9
β-actin
WT(Control)
KO(Control)
GFP/KO

◀ **Fig. 3** Comparison of liver fibrosis using TNFR1 KO mice. **a**, **b** anti-GFP immunohistochemistry (original magnifications, ×200). Both in wild type mouse live (**a**) and in TNFR1 KO mouse liver (**b**), the migrations of GFP positive bone marrow cells were confirmed. **c–f** Sirius red staining of liver sections (original magnifications, ×40). **g** Statistical analysis of fibrotic area. *Scale bars* standard deviations. Compared with WT (Control) (**c**), GFP/WT (**d**) had marked fibrolysis. KO (Control) (**e**) had significantly suppressed fibrosis but there was no marked improvement of fibrosis in GFP/KO (**f**). **h** Real-time RT-PCR analysis of expression of collagen type 1 alpha-1, indicating the fibrotic activity, showed similar results. **i–l** Immunohistochemistry of MMP-9 in liver sections (original magnifications, ×200). Liver section of WT (Control) (**i**) [magnified figure (×400) (**j**)] had certain degree of expression but in KO (Control) liver (**k**) and in GFP/KO liver (**l**), the expression was significantly low level. **m** Real-time RT-PCR analyses. **n** Western blot analyses of MMP-9; both showed suppression in TNFR1 KO mice but no significant increase in GFP/KO mice was seen and the suppression remained

phages were derived from differentiation and proliferation of recipient pre-existing cells (Fig. 4f).

Upregulation of TGF-β1 signals and hepatic stellate cell activation

Upon evaluation by immunostaining, TGF-β1 expression was decreased in KO (Control) mice but after BMC infusion, it was significantly increased (Fig. 4g–j). On real-time RT-PCR analysis as well, in KO mice, TGF-β1 increased after BMC infusion [KO (Control): GFP/KO, $p<0.05$] (Fig. 4k). On western blot analysis, the findings were similar (Fig. 4l). With alterations in TGF-β1 expression, stellate cell activity, evaluated by α-SMA staining, was suppressed in KO (Control) mice but with BMC infusion, in GFP/KO mice, it was significantly increased [KO (Control): GFP/KO, $p<0.05$] (Fig. 4m–p).

Discussion

TNF-α has long been known as an inflammatory cytokine whose action is mediated mainly by TNFR1. In addition to TNFR1, several other receptors exist, including TNFR2, each with a variety of actions, including cytotoxic effects, cell proliferation and protective effects. TNFR1 itself is known to be involved in various actions, including induction of hepatocyte apoptosis, extracellular matrix proliferation via downstream signals, anti-apoptosis effects and hepatocyte proliferation. In a previous partial hepatectomy model, the importance of TNF-α in liver regeneration was demonstrated (Yamada et al. 1997) but on the other hand, in studies using hepatotoxic factors such as CCl_4 and LPS, the involvement of TNF-α–TNFR1 pathways in the enhancement of liver cell injury and fibrosis has often been reported (Simeonova et al. 2001; Sudo et al. 2005; Horn et al. 2000). For applications of these findings to clinical liver disease, studies using TNFR1 knockout models, anti-TNF-α neutralizing antibodies and anti-TNFR1 antagonists have been conducted. Reductions in liver injury and liver fibrosis have been reported (Haak-Frendscho et al. 1994; Inui et al. 2005; Shibata et al. 2008a).

In the GFP/CCl_4 model, we reported that BMC infusion has liver repair effects and improves liver fibrosis (Terai et al. 2003). In reports to date from our laboratory, we have shown that inflammatory cytokines induced by CCl_4, primarily TNF-α, are important in BMC survival and liver repair (Omori et al. 2004). In addition, at other facilities, in vitro models have shown the importance of TNF-α signals in the differentiation of bone marrow stem cells to functional cells. There are various theories about BMC kinetics when infused in vivo (Higashiyama et al. 2007; Dalakas et al. 2009; Terai and Sakaida 2008; Khurana and Mukhopadhyay 2007) but much remains unknown.

In our study, to first confirm the effects of TNFR1, a TNFR1 antagonist was used. Because TNFR1 antagonists differ from anti-TNF-α antibodies, only block TNFR1, and do not affect other signal pathways such as TNFR2 (Shibata et al. 2008b), administration of a sufficient dose of antagonist in wild-type mice can reproduce a TNFR1 KO mouse system. A dose of 100 μg/body is sufficient to enable inhibition of intrahepatic inflammatory responses and liver fibrosis (Shibata et al. 2008a). Furthermore, the in vivo half-life of an intravenously administered TNFR1 antagonist is 5–6 days (Haak-Frendscho et al. 1994), so the blocking effect of TNFR1, up to the time of tissue sampling after 1 week, as used in the present protocol, probably continued.

In mice administered with the TNFR1 antagonist, intrahepatic macrophage infiltration was suppressed and stellate cell activation was decreased. Studies in liver injury suppression models, by inhibition of TNFα-TNFR1 signals, not only with TNFR1 antagonists but also with anti-TNF-α antibodies, have been reported by several facilities (Sudo et al. 2005; Yamada and Fausto 1998; Shibata et al. 2008a; Kitamura et al. 2002; Bahcecioglu et al. 2008). In the present study as well, in a model of advanced liver fibrosis induced by CCl_4 administration in wild-type mice, the TNFR1 antagonist suppressed intrahepatic inflammatory cell infiltration and improved liver fibrosis. However, in this model, with combined GFP-positive BMC infusion, intrahepatic inflammatory cell infiltration and stellate cell activation, which were suppressed by the antagonist, worsened with BMC infusion (attenuation of the suppression effect).

Next, to further clarify this phenomenon, TNFR1 KO mice were used as recipients to investigate whether there were differences in liver repair with BMC infusion based on the presence or absence of TNFR1. In GFP/KO mice, using TNFR1 KO mice as recipients, no liver repair effects with BMC infusion were observed. In TNFR1 KO mice,

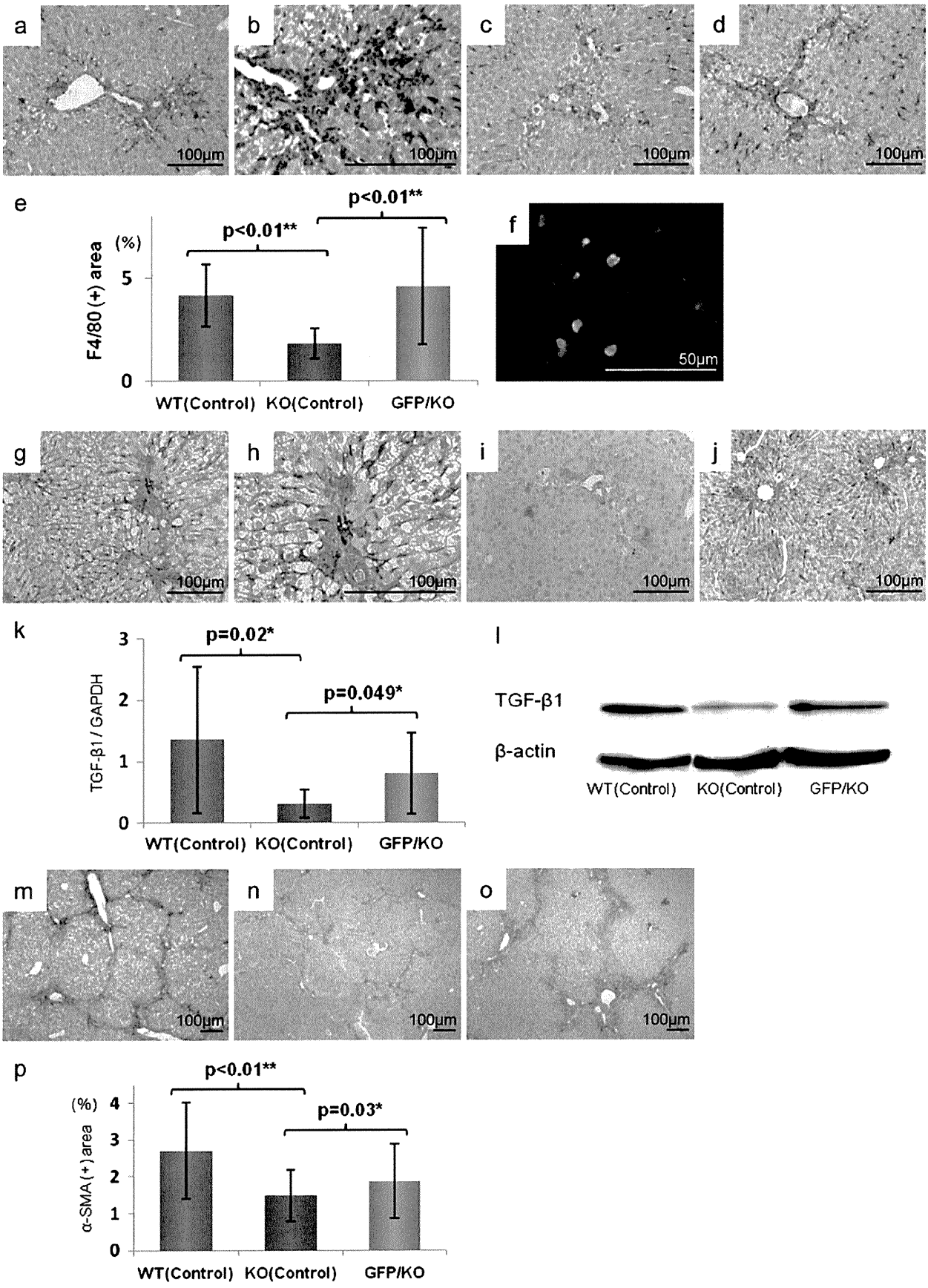
a
b
c
d
100μm
e
p<0.01**
p<0.01**
F4/80 (+) area (%)
5
0
WT(Control) KO(Control) GFP/KO
f
50μm
g
h
i
j
k
p=0.02*
p=0.049*
TGF-β1 / GAPDH
3
2
1
0
WT(Control) KO(Control) GFP/KO
l
TGF-β1
β-actin
WT(Control) KO(Control) GFP/KO
m
n
o
p
p<0.01**
p=0.03*
α-SMA (+) area (%)
4
3
2
1
0
WT(Control) KO(Control) GFP/KO

◀ **Fig. 4** Alteration of F4/80-positive cell infiltration, TGF-β1 expression and hepatic stellate cell activation. **a–d** Immunohistochemical analysis of F4/80 (original magnifications, ×100). **e** Statistical analysis of F4/80 positive area. *Scale bars* standard deviations. Compared with WT (Control) (**a**) [magnified figure (×200) (**b**)], the invasion of F4/80 positive cells was markedly suppressed in KO (Control) (**c**) and significantly increased in GFP/KO (**d**). **f** Double fluorescent immunohistochemistry of GFP and F4/80 (original magnifications, ×400). GFP was marked with FITC (*green*) and F4/80 with Cy3 (*red*). This showed the mismatch between the GFP-positive area and that of F4/80. **g–j** Immunohistochemical analyses of expression (original magnifications, ×100). WT (Control) (**g**) [magnified figure (×200) (**h**)] had much expression but in KO (Control) (**i**), it was suppressed. Adversely, GFP/KO (**j**) had more TGF-β1 expression than KO (Control). **k** Real-time RT-PCR analyses of TGF-β1. **l** Western blot analyses using TGF-β1 antibody. Both showed the increase of TGF-β1 expression in GFP/KO, suppressed in KO (Control). **m–o** Immunohistochemical analyses of α-SMA (original magnifications ×40). **p** Statistical analysis of α-SMA positive area. *Scale bars* standard deviations. Compared with WT (Control) (**m**), KO (Control) (**n**) had less hepatic stellate cell activation but the activation was markedly increased in GFP/KO (**o**)

compared to wild-type mice, although CCl_4-induced hepatotoxicity and liver fibrosis were suppressed, GFP-positive BMC infusion showed no synergism in liver repair or anti-hepatotoxic effects.

The importance of an increase in hepatic expression of MMP-9 by BMC infusion in liver fibrosis improvement has been reported by many facilities, including our laboratory (Sakaida et al. 2004, 2008; Higashiyama et al. 2007; Alwayn et al. 2008). In the present study, MMP-9 expression was markedly suppressed in TNFR1 KO mice compared to wild-type mice. MMP-9 expression has been shown to increase by TNF-α signals mediated via TNFR1 (Robinson et al. 2002; Vaday et al. 2001). In TNFR1 KO mice, the fact that this was suppressed is a consistent finding. In our laboratory, GFP-positive BMC infusion in wild-type mice was reported to enhance hepatic expression of MMP-9 (Sakaida et al. 2004). Within this series of cascades, inflammatory signals such as TNFR1 have been shown to be important (Omori et al. 2004). On the other hand, in GFP/KO mice, in which GFP-positive BMCs were infused in TNFR1 KO mice, there was no significant increase in MMP-9 expression and, moreover, the amount of expression compared to wild-type mice was significantly decreased, with no demonstrable effect on liver fibrolysis. With regard to the origin of MMP-9, infused BMCs have received attention but signals mediated by TNFR1 in pre-existing hepatocytes and host-derived hepatic macrophages are also important (Haruyama et al. 2000). These are suppressed in KO mice; furthermore, an increase in cytokine groups, such as increased TGF-β1 expression, which conversely suppresses MMP-9 expression, also has an influence (Vaday et al. 2001).

In TNFR1 KO mice, macrophage infiltration, increased TGF-β1 and enhanced α-SMA activity were noted. But no cells showing co-positivity with GFP staining were confirmed in F4/80 immunohistochemistry. We think the increase in macrophage came from recipient macrophage. In addition, as a result, other inflammatory signals such as TGF-β1 increased, followed by enhanced stellate cell activity and increased liver fibrosis (Parsons et al. 2007; Moreira 2007). DNA-Chip analysis also showed that the macrophage-related gene such as "monocyte-macrophage differentiation, MMD" was activated in TNFR1 KO mice by bone marrow cell infusion (data not shown). Several reports have evaluated the relationship between infiltrating macrophages in the liver with hepatotoxicity, liver fibrosis and liver regeneration (Liu et al. 2010; Duffield et al. 2005; Tacke et al. 2009). An association between intrahepatic macrophages with liver fibrolysis has also been reported (Fallowfield et al. 2007). Based on the present study, after BMC infusion in TNFR1 KO recipients, macrophages infiltrating the liver enhanced the above-mentioned inflammatory responses and increased liver fibrosis. In conclusion, proper TNFR1 signaling might be a key factor to induce the improvement of liver fibrosis by bone marrow cell infusion. Further studies will be needed to understand the precise mechanism.

Acknowledgements Ms. Mariko Yamada, Ms. Isako Fujimoto and Ms. Yoko Fukuzumi helped us with the cell culture and immunohistochemical analysis. This study was supported by Grants-in-Aid for scientific research from the Japan Society for the Promotion of Science (No. 22390150) and the Ministry of Health, Labour and Welfare, the Knowledge Cluster Initiative and Japan Science and Technology agency.

References

Alwayn I, Verbesey J, Kim S et al (2008) A critical role for matrix metalloproteinases in liver regeneration. J Surg Res 145:192–198

Bahcecioglu I, Koca S, Poyrazoglu O et al (2008) Hepatoprotective effect of infliximab, an anti-TNF-alpha agent, on carbon tetrachloride-induced hepatic fibrosis. Inflammation 31:215–221

Dalakas E, Newsome P, Boyle S, et al. (2009) Bone marrow stem cells contribute to alcohol liver fibrosis in humans. Stem Cells Dev

Drill V (1952) Hepatotoxic agents; mechanism of action and dietary interrelationship. Pharmacol Rev 4:1–42

Duffield J, Forbes S, Constandinou C et al (2005) Selective depletion of macrophages reveals distinct, opposing roles during liver injury and repair. J Clin Invest 115:56–65

Fallowfield JA, Mizuno M, Kendall TJ et al (2007) Scar-associated macrophages are a major source of hepatic matrix metalloproteinase-13 and facilitate the resolution of murine hepatic fibrosis. J Immunol 178:5288–5295

Gardner C, Laskin J, Dambach D et al (2003) Exaggerated hepatotoxicity of acetaminophen in mice lacking tumor necrosis factor receptor-1. Potential role of inflammatory mediators. Toxicol Appl Pharmacol 192:119–130

Haak-Frendscho M, Marsters S, Mordenti J et al (1994) Inhibition of TNF by a TNF receptor immunoadhesin. Comparison to an anti-TNF monoclonal antibody. J Immunol 152:1347–1353

Haruyama T, Ajioka I, Akaike T et al (2000) Regulation and significance of hepatocyte-derived matrix metalloproteinases in liver remodeling. Biochem Biophys Res Commun 272:681–686

Higashiyama R, Inagaki Y, Hong Y et al (2007) Bone marrow-derived cells express matrix metalloproteinases and contribute to regression of liver fibrosis in mice. Hepatology 45:213–222

Horn T, O'Brien T, Schook L, Rutherford M (2000) Acute hepatotoxicant exposure induces TNFR-mediated hepatic injury and cytokine/apoptotic gene expression. Toxicol Sci 54:262–273

Inui T, Nakashima H, Habu Y et al (2005) Neutralization of tumor necrosis factor abrogates hepatic failure induced by alpha-galactosylceramide without attenuating its antitumor effect in aged mice. J Hepatol 43:670–678

Khurana S, Mukhopadhyay A (2007) Characterization of the potential subpopulation of bone marrow cells involved in the repair of injured liver tissue. Stem Cells 25:1439–1447

Kitamura K, Nakamoto Y, Akiyama M et al (2002) Pathogenic roles of tumor necrosis factor receptor p55-mediated signals in dimethylnitrosamine-induced murine liver fibrosis. Lab Invest 82:571–583

Liu C, Tao Q, Sun M et al (2010) Kupffer cells are associated with apoptosis, inflammation and fibrotic effects in hepatic fibrosis in rats. Lab Invest 90:1805–1816

Moreira R (2007) Hepatic stellate cells and liver fibrosis. Arch Pathol Lab Med 131:1728–1734

Omori K, Terai S, Ishikawa T et al (2004) Molecular signature associated with plasticity of bone marrow cell under persistent liver damage by self-organizing-map-based gene expression. FEBS Lett 578:10–20

Parsons CJ, Takashima M, Rippe RA (2007) Molecular mechanisms of hepatic fibrogenesis. J Gastroenterol Hepatol 22(Suppl 1):S79–S84

Pfeffer K, Matsuyama T, Kunding TM et al (1993) Mice deficient for the 55 kd tumor necrosis factor receptor are resistant to endotoxic shock, yet succumb to L. monocytogenes infection. Cell 73:457–467

Robinson S, Scott K, Balkwill F (2002) Chemokine stimulation of monocyte matrix metalloproteinase-9 requires endogenous TNF-alpha. Eur J Immunol 32:404–412

Sakaida I (2008) Autologous bone marrow cell infusion therapy for liver cirrhosis. J Gastroenterol Hepatol 23:1349–1353

Sakaida I, Terai S, Yamamoto N et al (2004) Transplantation of bone marrow cells reduces CCl4-induced liver fibrosis in mice. Hepatology 40:1304–1311

Shibata H, Yoshioka Y, Ohkawa A et al (2008a) The therapeutic effect of TNFR1-selective antagonistic mutant TNF-alpha in murine hepatitis models. Cytokine 44:229–233

Shibata H, Yoshioka Y, Ohkawa A et al (2008b) Creation and X-ray structure analysis of the tumor necrosis factor receptor-1-selective mutant of a tumor necrosis factor-alpha antagonist. J Biol Chem 283:998–1007

Simeonova P, Gallucci R, Hulderman T et al (2001) The role of tumor necrosis factor-alpha in liver toxicity, inflammation, and fibrosis induced by carbon tetrachloride. Toxicol Appl Pharmacol 177:112–120

Sudo K, Yamada Y, Moriwaki H, Saito K et al (2005) Lack of tumor necrosis factor receptor type 1 inhibits liver fibrosis induced by carbon tetrachloride in mice. Cytokine 29:236–244

Tacke F, Luedde T, Trautwein C (2009) Inflammatory pathways in liver homeostasis and liver injury. Clin Rev Allergy Immunol 36:4–12

Terai S, Sakaida I (2008) Current status of autologous bone marrow cell infusion therapy for liver cirrhosis patients. Hepatol Res 38: S72–S75

Terai S, Yamamoto N, Omori K et al (2002) A new cell therapy using bone marrow cells to repair damaged liver. J Gastroenterol 37 (Suppl 14):162–163

Terai S, Sakaida I, Yamamoto N et al (2003) An in vivo model for monitoring trans-differentiation of bone marrow cells into functional hepatocytes. J Biochem 134:551–558

Terai S, Sakaida I, Nishina H et al (2005) Lesson from the GFP/CCl4 model–translational research project: the development of cell therapy using autologous bone marrow cells in patients with liver cirrhosis. J Hepatobiliary Pancreat Surg 12:203–207

Vaday G, Schor H, Rahat M et al (2001) Transforming growth factor-beta suppresses tumor necrosis factor alpha-induced matrix metalloproteinase-9 expression in monocytes. J Leukoc Biol 69:613–621

Yamada Y, Fausto N (1998) Deficient liver regeneration after carbon tetrachloride injury in mice lacking type 1 but not type 2 tumor necrosis factor receptor. Am J Pathol 152:1577–1589

Yamada Y, Kirillova I, Peschon J et al (1997) Initiation of liver growth by tumor necrosis factor: deficient liver regeneration in mice lacking type I tumor necrosis factor receptor. Proc Natl Acad Sci USA 94:1441–1446

Cell Tissue Res (2011) 344:125–134
DOI 10.1007/s00441-011-1132-7

REGULAR ARTICLE

Telmisartan improves nonalcoholic steatohepatitis in medaka (*Oryzias latipes*) by reducing macrophage infiltration and fat accumulation

Shinya Kuwashiro · Shuji Terai · Toshiyuki Oishi · Koichi Fujisawa · Toshihiko Matsumoto · Hiroshi Nishina · Isao Sakaida

Received: 7 September 2010 / Accepted: 12 January 2011 / Published online: 16 February 2011

Abstract We investigated the efficacy of the antihypertensive drug telmisartan (Tel) and the mechanisms underlying the progression from simple steatosis to nonalcoholic steatohepatitis (NASH) in a medaka (*Oryzias latipes*) NASH model. We used the NASH activity score (NAS) developed in humans to assess the histology of the medaka NASH model and found that NAS increased with time. Further, TUNEL-positive apoptosis hepatocytes were found in the medaka NASH model. Tel administration resulted in the increased expression of liver peroxisome proliferator-activated receptor-γ, carnitine palmitoyltransferase 1 and acyl-CoA oxidase 1 and decreased the number of 8-hydroxydeoxyguanosine-positive hepatocytes and the migration of macrophages positive for diastase-periodic-acid-Schiff. Medaka NAS was improved by Tel administration but fatty acid content was not affected. Tel reduced the infiltration of macrophages into the liver and ameliorated NASH pathology.

Keywords Nonalcoholic steatohepatitis · Telmisartan · Macrophage · Apoptosis · Medaka · Oryzias latipes (Teleostei)

Abbreviations

ACC	acetyl CoA carboxylase
ACO	acyl-CoA oxidase
BMI	body mass index
CCR2	CC chemokine receptor 2
CPT	carnitine palmitoyltransferase
D-PAS	diastase-periodic-acid-Schiff
FAS	fatty acid synthase
HE	haematoxylin and eosin
HFD	high-fat diet
MCP1	monocyte chemotactic protein 1
MNAS	medaka NAS
NAFLD	nonalcoholic fatty liver disease
NAS	NAFLD activity score
NASH	nonalcoholic steatohepatitis
8-OHdG	8-hydroxydeoxyguanosine
PB	phosphate buffer
PCR	polymerase chain reaction
PPAR	peroxisome proliferator-activated receptor
PUFA	polyunsaturated fatty acid
RT	real-time
Tel	telmisartan
TG	triglyceride

Financial support This study was supported by Grants-in-Aid for Scientific Research from the Japan Society for the Promotion of Science (nos. 18590737 18659209, 19590693, 19390199, 20659116, 21659189), the Knowledge Cluster Initiative, Japan, the Aerospace Exploration agency (JAXA), the Ministry of Health, Labour and Welfare and the Japan Science and Technology agency.

The authors have no competing interests to declare.

S.K., S.T. and I.S. conceived and designed the experiments. T.M., S. K., K.F., T.O. and N.Y. performed the experiments. T.M., Y.F. and Y. H. analyzed the data. M.F and H.N. contributed reagents/materials/ analysis tools. S.K. and S.T. wrote the paper.

S. Kuwashiro · S. Terai (✉) · T. Oishi · K. Fujisawa · T. Matsumoto · I. Sakaida
Department of Gastroenterology and Hepatology, Yamaguchi University Graduate School of Medicine, Minami Kogushi 1-1-1, Ube, Yamaguchi 755-8505, Japan
e-mail: terais@yamaguchi-u.ac.jp

H. Nishina
Department of Developmental and Regenerative Biology, Medical Research Institute, Tokyo Medical and Dental University, 1-5-45 Yushima, Bunkyo-ku, Tokyo 113-8510, Japan

Introduction

The number of patients worldwide with nonalcoholic fatty liver disease (NAFLD) has been increasing in recent years. NAFLD is defined as fatty liver (steatosis) occurring in the absence of a history of alcohol abuse. NAFLD is closely linked to obesity, diabetes, hyperlipidaemia and insulin resistance and is considered to represent a hepatic manifestation of metabolic syndrome (Powell et al. 1990; Sanyal 2002). NAFLD can be classified into either nonprogressive simple steatosis or nonalcoholic steatohepatitis (NASH) with inflammation, ballooning degeneration and fibrosis (Schaffner and Thaler 1986; Younossi et al. 1998). NASH is a progressive chronic liver disease that can develop into cirrhosis of the liver and liver cancer; it occurs with high frequency in obese individuals and in type 2 diabetes patients and is thought to represent a hepatic manifestation of metabolic syndrome. No effective treatments have yet been established for NASH, and the mechanisms underlying the progression from simple steatosis to NASH have not been fully clarified.

Previous studies of NASH have made extensive use of murine models such as mice or rats but the use of small fish such as zebrafish (*Danio rerio*) is now common. Medaka (*Oryzias latipes*) is a small fish, like zebrafish (Chu and Chiu 2008; Terai 2010), that is found in Japan and continental Asia. Numerous pure medaka bloodlines have been used in Japan as model animals (Masahito et al. 1989). Compared with murine models, medaka is highly fecund, rapidly maturing, and small, thus reducing cost and space requirements. Further, the mapping of the medaka genome has been completed and methods for producing transgenic and knockout individuals have been established, fulfilling the requirements of an animal model (Kasahara et al. 2007). We have previously observed that feeding medaka a high-fat diet (HFD) results in liver histology resembling that of human NASH and we have reported this as a novel medaka NASH model (Matsumoto et al. 2010). Administration of n3 polyunsaturated fatty acids (n3 PUFAs) to this medaka NASH model ameliorates steatosis, indicating that this model is useful for the investigation of drug effectiveness (Matsumoto et al. 2010). Mutant lines with liver steatosis have been developed in zebrafish (*foie gras* mutant) and medaka (*Kendama* mutant) with forward genetic screening by using N-ethyl-N-nitrosourea treatment (Sadler et al. 2005; Watanabe et al. 2004). Medaka fish and zebrafish will be good models for the analysis of NASH pathology but, at present, our developed medaka NASH model is the only one to show similarity with human NASH (Matsumoto et al. 2010).

In the present study, we have used the medaka NASH model to investigate the efficacy of the antihypertensive drug telmisartan (Tel). This drug blocks angiotensin II type 1 receptors, excites peroxisome proliferator-activated receptor (PPAR)-γ and has been reported to improve glycolipid metabolism. We have also found that Tel administration ameliorates hepatic fibrosis induced in a model fed with a choline-deficient L-amino-acid-defined diet (Jin et al. 2007). NASH progression can be evaluated in clinical settings by means of the NAFLD activity score (NAS); this score (more precisely termed the medaka NAS; MNAS) has been employed in the present study to examine the pathological condition presented by NASH and to clarify changes in this condition. We have used the medaka NASH model to investigate the involvement of macrophages in the progression of NASH pathology.

Materials and methods

Animals and diets

Himedaka Cab fish (an orange-red variety of medaka) at 8 weeks old were used for most experiments. Fish were maintained in accordance with the Animal Care Guidelines of Yamaguchi University. During experiments, fish in groups of 10 were kept in tap water in plastic tanks covered with plastic covers and illuminated with fluorescent light from 08:00 to 22:00. Temperature was controlled at 26±1°C. Each tank was supplied with 200 mg food, daily, and all provided food was consumed within 14 h. The energy content of the control diet (Hikari Crest; Kyorin, Hyogo, Japan) was 3.3 kcal/g with 25.3% from fat, 62.5% from protein and 13.8% from carbohydrates, plus vitamins and minerals as recommended. The energy content of the HFD (HFD32; CLEA Japan, Tokyo, Japan) was 5.1 kcal/g with 56.7% from fat, 20.1% from protein and 23.2% from carbohydrates, plus vitamins and minerals as recommended. The fatty acid composition was as shown previously with a ratio of n3/n6 PUFAs of 0.02 (Matsumoto et al. 2010). Tel was dissolved in dimethyl sulfoxide to a concentration of 2 mg/ml prior to administration to the test tank at a final concentration of 1 mg/l.

Tissue collection and histology

Fish were killed and opened from the anal vent to the gills. The entire body was fixed with 4% paraformaldehyde in 0.1 M phosphate buffer (PB). The liver was dissected, dehydrated in alcohol and embedded in paraffin according to routine procedures. Serial sections were made at a thickness of 3-5 μm. Staining was performed by using haematoxylin and eosin (HE). The number of diastase-periodic-acid-Schiff (D-PAS)-positive cells per liver section (a single field of view at 400× magnification) was used to assess macrophage infiltration with inflammation (Brunt 2001).

Immunohistochemical examination and TUNEL assay

CD68 as a marker for macrophages and 8-hydroxydeoxyguanosine (8-OHdG) for the detection of oxidative stress were immunohistochemically assessed by using the avidin-biotin-peroxidase complex method, as described previously (Kolak et al. 2007; Sakaida et al. 1994). The TUNEL (terminal deoxynucleotidyl transferase-mediated dUTP nick-end labelling) assay was performed by using a commercially available kit (In Situ Cell Death Detection Kit; Roche Diagnostics, Indianapolis, Ind., USA) according to the manufacturer's instructions. Hepatocyte apoptosis in liver sections was quantified by counting the number of TUNEL-positive cells in random microscopic low-power fields (×100).

Blood analysis

Blood samples were obtained from medaka following a 12-h fast. Fish were kept on ice for 1–2 min and then bled by cutting a ventral portion of the tail fin. Blood was collected in a microcapillary tube and the collected volume was measured. Blood samples were kept at room temperature for 1 h before centrifugation at 1200*g* for 30 min at 4°C. Serum triglyceride concentrations were measured by using a Fuji Drychem 3500 auto-analyser (Fujifilm, Tokyo, Japan). Cholesterol and triglyceride (TG) profiles in total lipoproteins were analysed by means of a dual-detection high-performance liquid chromatography system with two tandem-connected TSK gel LipopropakXL columns (300×7.8 mm; Tosoh, Tokuyama, Japan) by Skylight Biotech (Akita, Japan).

Fatty acid analysis

The fatty acid composition of homogenized liver tissue (20 mg tissue/ml saline) was determined by capillary gas chromatography. Total lipids were extracted by using the procedure described by Folch et al. (1957) and fatty acids were methylated with boron trifluoride and methanol. Methylated fatty acids were analysed by using a GC-17A gas chromatograph (Shimadzu, Kyoto, Japan) equipped with a BPX70 capillary column (0.25 mm internal diameter×30 mm; SGE International, Melbourne, Australia). Tricosanoic acid (C23:0) was used as the internal standard. The minimum detectable fatty acid concentration detected by this assay was 0.5 μg/ml.

Semi-quantitative real-time polymerase chain reaction

To avoid the acute effects of food intake, fish were fasted overnight prior to being killed. Total RNA was extracted from resections of the liver and purified by using the RNeasy kit (Qiagen, Hilden, Germany). Next, cDNAs were synthesized by using purified RNA with random hexamers in the Transcriptor First Strand cDNA synthesis kit (Roche, Indianapolis, Ind., US). Semi-quantitative real-time (RT) polymerase chain reaction (PCR) was performed with PCR master mix (Promega, Madison, Wis., US) and the primers are listed in Table 1. Gene expression levels were normalized against β-actin as an endogenous positive control; acetyl-CoA carboxylase (ACC) 1, carnitine palmitoyltransferase (CPT) 1, acyl CoA oxidase (ACO) 1, PPAR-γ and fatty acid synthase (FAS) were analysed.

Statistical analyses

Numerical data are expressed as the mean±standard deviation. Student's *t*-test was performed to assess statistical significance among treatment groups. Differences were considered significant at $P<0.05$.

Results

Development of steatosis and inflammation of liver tissue in medaka NASH model and NAS evaluation

Medaka in the HFD group had a higher body weight and body mass index (BMI) than the control group fed on a normal diet. Gross evaluation of the liver showed a whitish hue developing over time in the HFD group (Fig. 1). Hepatic steatosis was assessed by scoring HE-stained liver sections. A three-stage scoring system was used: mild (score 1), fat development confined to the areas surrounding blood vessels; moderate (score 2), midway between mild and

Table 1 Lists of primers for selected genes (*ACC1* acetyl-CoA carboxylase 1, *ACO1* acyl CoA oxidase 1, *CPT1* carnitine palmitoyltransferase 1, *FAS* fatty acid synthase, *PPAR-γ* peroxisome proliferator-activated receptor-γ)

Gene	Forward primer (5′ to 3′)	Reverse primer (3′ to 5′)
ACC1	GAGTGACGTCCTGCTTGACA	ACCTTTGGTCCACCTCACAG
ACO1	GCTCAGCTTTACAGCCTTGG	GGACGATTCCCTAACGATCA
CPT1	ATGTCTACCTCCGTGGACGA	CAAGTTTGGCCTCTCCTTTG
FAS	GACGCTTCAGGAAATGGGTA	GGACAGGAACCGGACTATCA
PPAR-γ	ACGCTTCCATTTCCTCCTCT	GACAGTGAAGGTCGCAGTGA
β-Actin	CTGGACTTCGAGCAGGAGAT	GCTGGAAGGTGGACAGAGAG

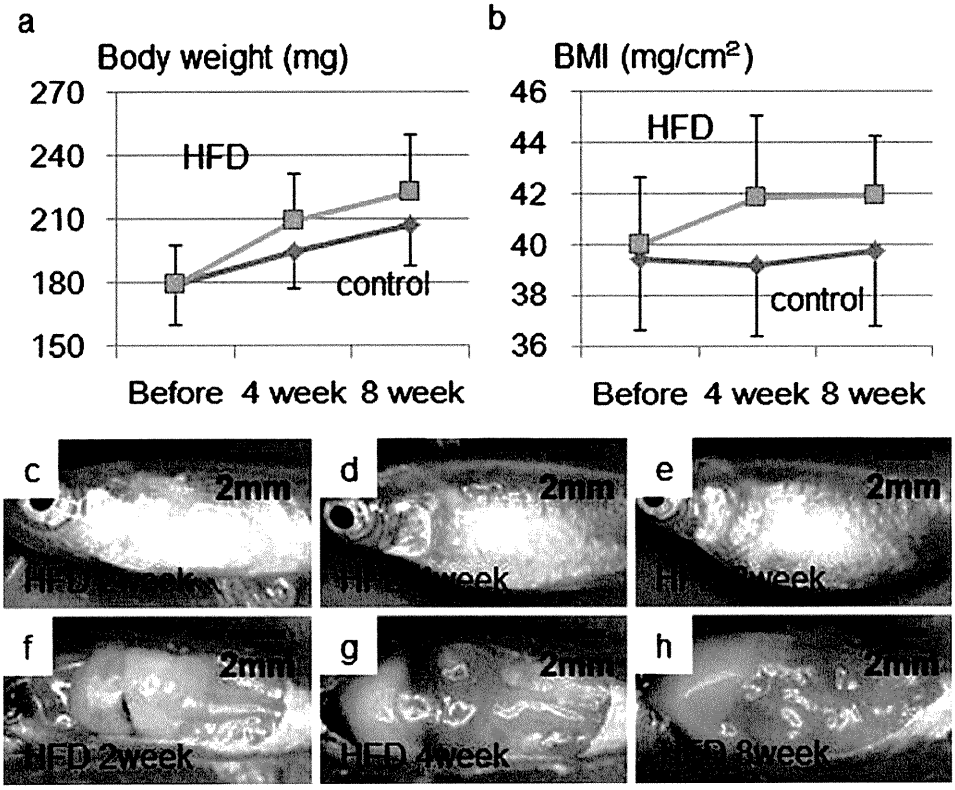

Fig. 1 The high-fat diet (*HFD*) group showed a higher body weight(**a**) and body mass index (*BMI*; **b**) than the normal diet (*control*) group as a result of the high fat intake. In the HFD group, distention of the abdomen increased (**c-e**) and the liver showed a more noticeable whitish hue (**f-h**) over time

severe; severe (score 3), diffuse hepatic steatosis. The score after 4 weeks of HFD administration was 1.5±0.8, which increased to 2.6±0.8 after 8 weeks, indicating the progression of steatosis. The number of D-PAS-positive cells was 0.6±0.2 after 4 weeks of HFD administration and reached 4.7±1.3 after 8 weeks, showing a clear increase in inflammatory cell infiltration (Fig. 2a-h).

In clinical settings, the recommendation has been made to distinguish NASH from simple steatosis by using the findings of NAS, which is based on the degree of steatosis, hepatocyte ballooning and lobular inflammation. We adapted NAS to medaka by employing the MNAS (scoring criteria summarized in Table 2). Steatosis was scored according to the three-stage scoring system described above. Lobular inflammation was scored by assigning a score scheme according to the number of D-PAS-positive cells per tissue section (single field of view at 400× magnification). Hepatocyte ballooning was scored as 1 for a small number of cells showing ballooning and 2 for a marked number of cells showing ballooning. MNAS was 1.9±0.7 after 4 weeks of HFD administration and 4.9±1.5 after 8 weeks, showing a clear increase over time (Fig. 2i).

Tel suppresses weight gain in the medaka NASH model

Compared with the HFD group, a lower weight gain was observed in the Tel group. Likewise, the increase in BMI was less in the Tel group. A comparison of the gross appearance of the liver also showed less steatosis in the Tel group than in the HFD group (Fig. 3).

Tel suppresses development of steatosis and inflammation in the medaka NASH model and improves MNAS

The histological investigation revealed the deposition of lipid droplets in hepatocytes after 2 weeks, with lipid deposition becoming striking and clear cell formation being found after 4 weeks on the HFD. Degenerated hepatocytes were found at 8 weeks. In the Tel group with administration at 1 ppm, hepatic steatosis was reduced. No mortality or effects on mobility were found in the Tel group (Fig. 4a-f). Compared with the HFD group, the Tel group showed ameliorated steatosis and inflammatory cell infiltration. MNAS was significantly improved in the Tel group (1.6±0.9 after 4 weeks, 3.8±1.0 after 8 weeks) compared with the HFD group (1.9±0.7 after 4 weeks, 4.9±1.5 after 8 weeks; Fig. 4g).

Blood examination in the medaka NASH model

Measurement of blood levels of TG in the control, HFD and Tel groups at 4 and 8 weeks showed that TG increased over time in the HFD and Tel groups compared with the control group (Table 3). The TG level was slightly higher in

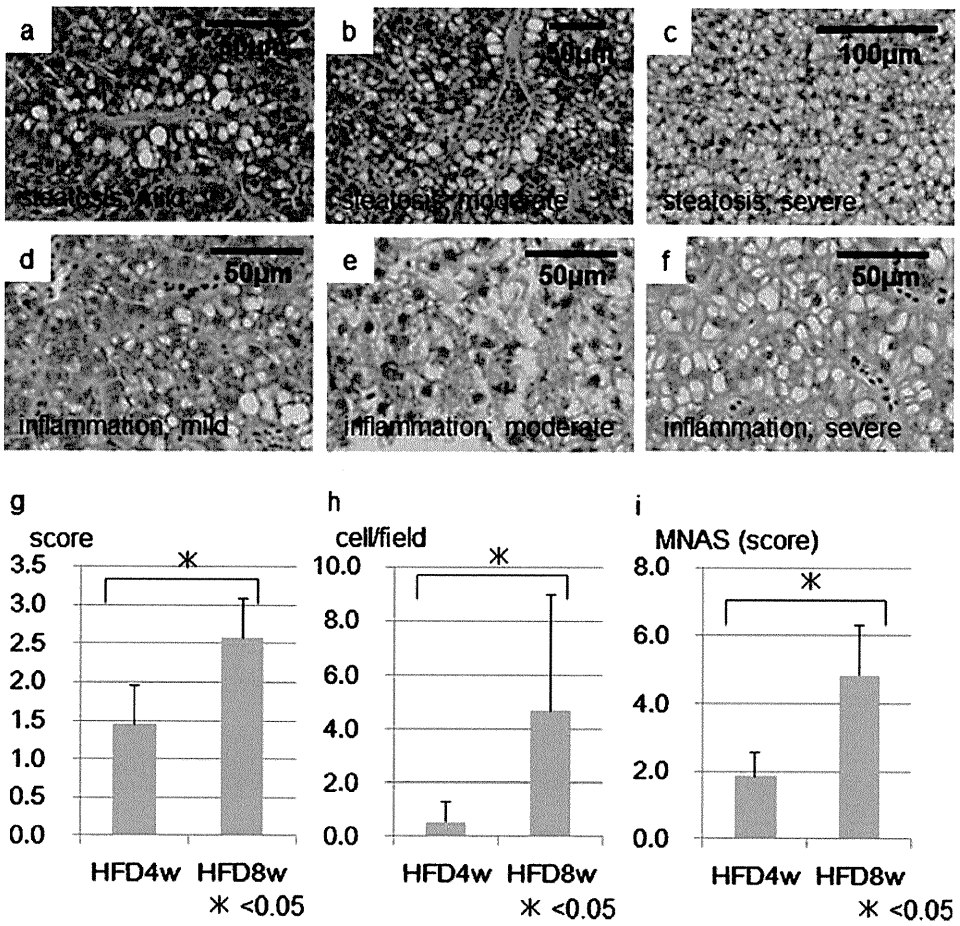

Fig. 2 Histological analysis for nonalcoholic steatohepatitis (NASH) medaka. Hepatic steatosis was assessed by scoring sections of liver stained by haematoxylin and eosin (HE) on a three-stage scoring system: mild (score 1; **a**); moderate (score 2; **b**); severe diffuse (score 3; **c**). After 4 weeks of HFD, the score was 1.5±0.8, increasing to 2.6±0.8 after 8 weeks, thereby indicating steatosis progression ($P<0.05$; **g**). D-PAS staining was used to assess inflammatory cell infiltration according to the number of D-PAS-positive cells per tissue section (a single field of view at 400× magnification; *$P<0.05$; **d-f**, **h**). The medaka NAS (MNAS) was 1.9±0.7 after 4 weeks of HFD administration and 4.9±1.5 after 8 weeks, showing a clear increase in the score over time (*$P<0.05$; **i**). The scoring system for the three parameters is summarized in Table 2

the Tel group than in the HFD group (Fig. 5a). The HFD and Tel groups both showed clear increases in the amount of fatty acids in the liver at 4 weeks compared with the control group. The n3/n6 PUFA ratio was lower in the HFD and Tel groups than in the control group at 4 weeks but no differences were observed in the n3/n6 PUFA ratio between the HFD and Tel groups (Table 4).

Table 2 Critera for nonalcoholic fatty liver disease (NAFLD) activity score (*NAS*) in medaka

Parameter	Definition	NAS
Steatosis	None	0
	Mild	1
	Moderate	2
	Severe	3
Inflammation	×400 0-1	0
	×400 2-3	1
	×400 4-5	2
	×400 5 or greater	3
Ballooning	None	0
	Several	1
	Large number	2

Macrophage infiltration and oxidative stress in medaka NASH liver tissue

D-PAS staining indicated that both inflammatory cells and macrophages in the liver tissue of the medaka NASH model increased over time on HFD (Fig. 2h). Furthermore, we observed tissue with locally aggregated hepatocyte degeneration in some areas of medaka NASH model liver tissue. D-PAS-positive cells were found at each location, with CD68-positive cells at ballooning hepatocyte foci (Fig. 5b-d). The HFD group showed many cells with 8-OHdG-positive nuclei (Fig. 5e, f). Hepatocyte degeneration resembling cell ballooning, inflammatory cell (macrophage) infiltration at the same location and oxidative stress were confirmed as the constituent elements of NASH pathology in medaka NASH model liver tissue. A reduced number of CD68-positive cells, indicating a reduction in oxidative stress, was detected in the Tel group.

Induction of apoptosis in medaka steatohepatic liver

The number of apoptotic cells was greater in the HFD group than in the control group from 4 weeks as shown

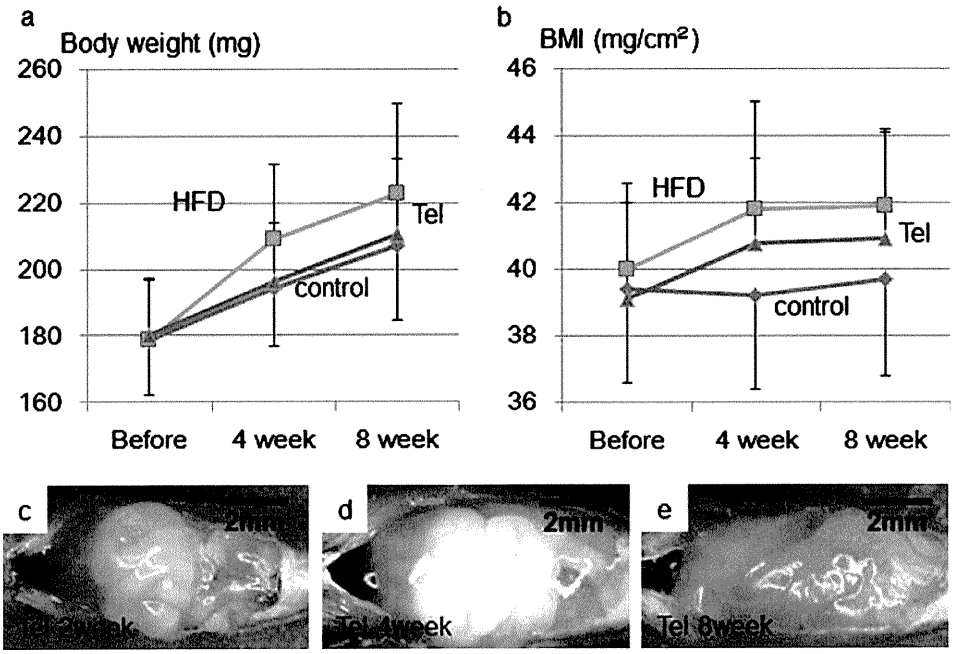

Fig. 3 Weight gain in the telmisartan (Tel) group was attenuated compared with that in the HFD group (**a**). Likewise, the BMI increase was also attenuated in the Tel group compared with the HFD group (**b**). A comparison of the gross appearance of livers also showed less steatosis in the Tel group (**c–e**) than in the HFD group (Fig. 1c-h)

by TUNEL staining (Fig. 6). Apoptotic cells were observed mainly in the vicinity of blood vessels, such as the portal veins and other veins, and fewer apoptotic cells were seen in the Tel group than in the HFD group.

Changes in gene expression

With regard to the mode of action of Tel on the liver, PPAR-γ mRNA expression increased in the Tel group (Fig. 7). RT-PCR analysis showed changes in expression for some genes involved in glycolipid metabolism and the pathway for de novo synthesis of fatty acids. The expression of FAS showed no clear changes in the HFD or Tel groups compared with the control group (Fig. 7), whereas the ACC1 genes showed reduced expression in both the HFD and Tel groups compared with the control group. The expression of CPT1, indicating β-oxidation in the mitochondria, was higher in the HFD group than in the control group and was higher still in the Tel group. The expression of ACO1, indicating β-oxidation in the peroxisomes, was lower in the HFD group than in the control group but similar levels of expression were seen in the Tel and control groups.

Discussion

We have previously reported the creation of a new NASH model by feeding medaka with an HFD and its use as a valid model for screening drugs (Matsumoto et al. 2010). In the present study, we were able to confirm that medaka fed HFD showed inflated abdomens and white liver and developed NASH liver (Fig. 1). Histologically, lipid droplet deposition was found in medaka hepatocytes from 2 weeks and became more marked with inflamed and degenerated hepatocytes being present from 4 weeks (Fig. 4). These results suggested that the medaka model was easily affected by diet itself. Next, we made a histological assessment of medaka liver tissue according to MNAS, based on NAS, a classification system for human NAFLD/NASH pathology in clinical settings (Kleiner et al. 2005). We confirmed that MNAS increased over time in the medaka NASH model. Moreover, liver tissue in the medaka NASH model showed fat deposition in hepatocytes and, if the hepatocyte degeneration was interpreted as ballooning, the NAFLD pathology could be assessed as type 3 according to the criteria of Matteoni et al. (1999) and could be regarded as being equivalent to the human NASH histology.

In our study, we have used this model to investigate the effects of Tel, an antihypertensive drug that acts as a partial antagonist of PPAR-γ, which has been reported to improve glycolipid metabolism. Tel has been reported to attenuate body weight gain and control fatty liver in rat and mouse NASH models (Benson et al. 2004; Schupp et al. 2005). We have performed gene expression analysis by using RT-PCR on medaka liver and found that PPAR-γ gene expression in the liver is accelerated by Tel administration. This confirms that Tel also stimulates PPAR-γ in medaka (Fig. 7). NASH pathology in medaka is ameliorated by Tel administration (Figs. 1-6), although no changes in the levels of TG or very low-density lipoprotein have been found in medaka blood. We have previously shown that n3 PUFA administration ameliorates medaka NASH and the n3/n6 PUFA ratio imbalance in liver fatty acid fractions; however, Tel

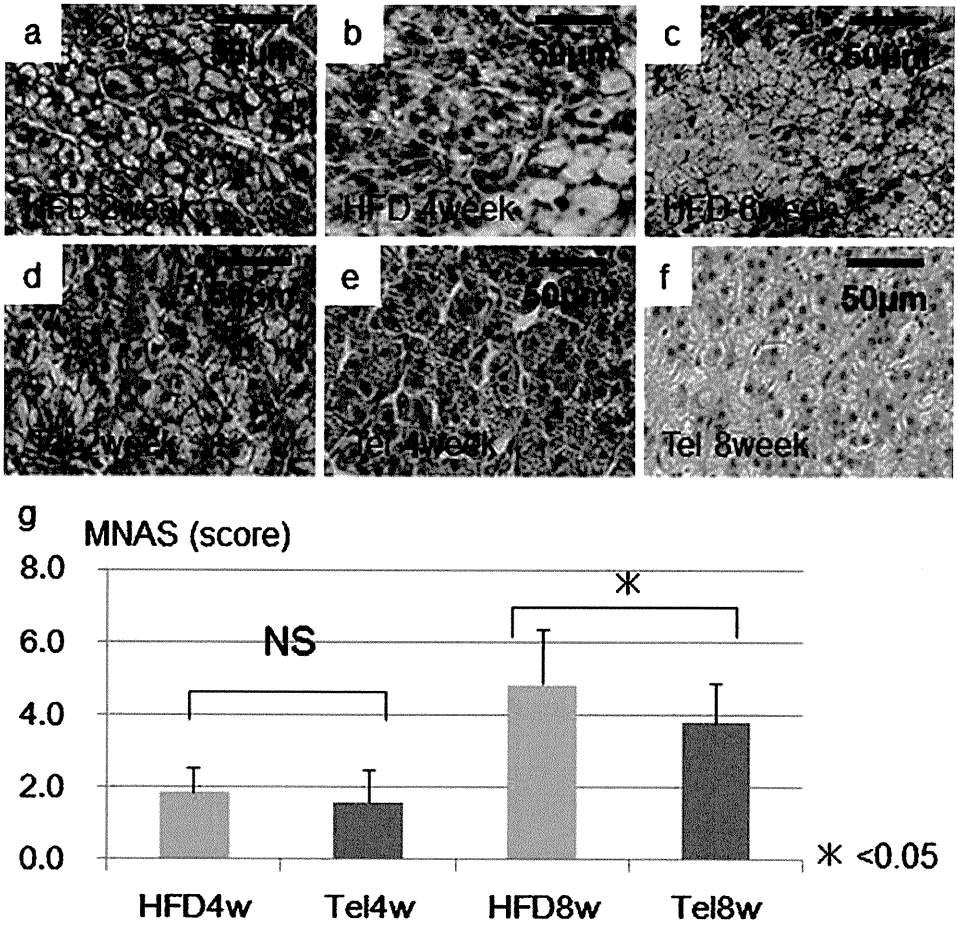

Fig. 4 Medaka histology demonstrated lipid droplet deposition in hepatocytes after 2 weeks of HFD (**a**). Lipid deposition in hepatocytes was striking and clear cell formation was observed after 4 weeks (**b**). Degenerated hepatocytes were seen at 8 weeks (**c**). In the Tel group (1 ppm), hepatic steatosis was attenuated over the same period (**d–f**). In terms of MNAS, a significant difference was seen between the Tel group (1.6±0.9 after 4 weeks [*Tel4w*], 3.8±1.0 after 8 weeks [*Tel8w*], $P<0.05$) and the HFD group (1.9±0.7 after 4 weeks [*HFD4w*], 4.9±1.5 after 8 weeks [*HFD8w*], $P<0.05$) with the Tel group showing improved MNAS (Tel group after 8 weeks at 3.8±1.0 vs HFD group after 8 weeks at 4.9±1.5; $*P<0.05$; *NS* nonsignificant; **g**)

administration in the present study does not seem to ameliorate the n3/n6 PUFA ratio imbalance in the liver (Table 4). Ballooning degeneration is assumed to be related to changes in the lipid composition of the fatty acid bilayer in the cellular membrane and to the n3/n6 PUFA ratio. Although no change in the n3/n6 PUFA ratio of the liver fatty acid fraction attributable to Tel administration has been found, Tel ameliorates ballooning degeneration.

The medaka NASH model shows increased liver tissue infiltration by D-PAS-positive and CD68-positive macrophages over time from the start of HFD (Figs. 2, 5b-c) but such cellular infiltrations are suppressed by Tel administration. These results suggest that the ballooning degeneration of hepatocytes might be closely regulated by macrophage infiltration. More detailed investigations of the relationship between ballooning degeneration and changes in the lipid composition of the fatty acid bilayer in the cellular membrane are needed.

These observations indicate that progression of NASH pathology is linked to the infiltration of macrophages into liver tissue and that Tel is effective as a dietary treatment to suppress such infiltration. A recent study has suggested that an increase in the number of macrophages infiltrating adipose tissue is correlated with obesity (Weisberg et al. 2003). Activated monocytes have been found in the arterial walls of humans and other animals with hypertension (Ishibashi et

Table 3 Triglyceride (mg/dl) changes in medaka blood (1 sample=10 fish; *HFD* high-fat diet, *Tel* telmisartan, *w* week)

Treatment	Total	Chylomicron	Very low-density lipoprotein	Low-density lipoprotein	High-density lipoprotein
Normal	407.4	6.0	107.9	38.4	255.1
HFD4w	955.9	179.6	353.0	65.0	358.2
HFD8w	1352.9	303.4	571.8	107.3	370.5
Tel4w	1035.1	188.1	403.2	91.3	352.6
Tel8w	1490.8	267.3	649.0	133.8	440.7

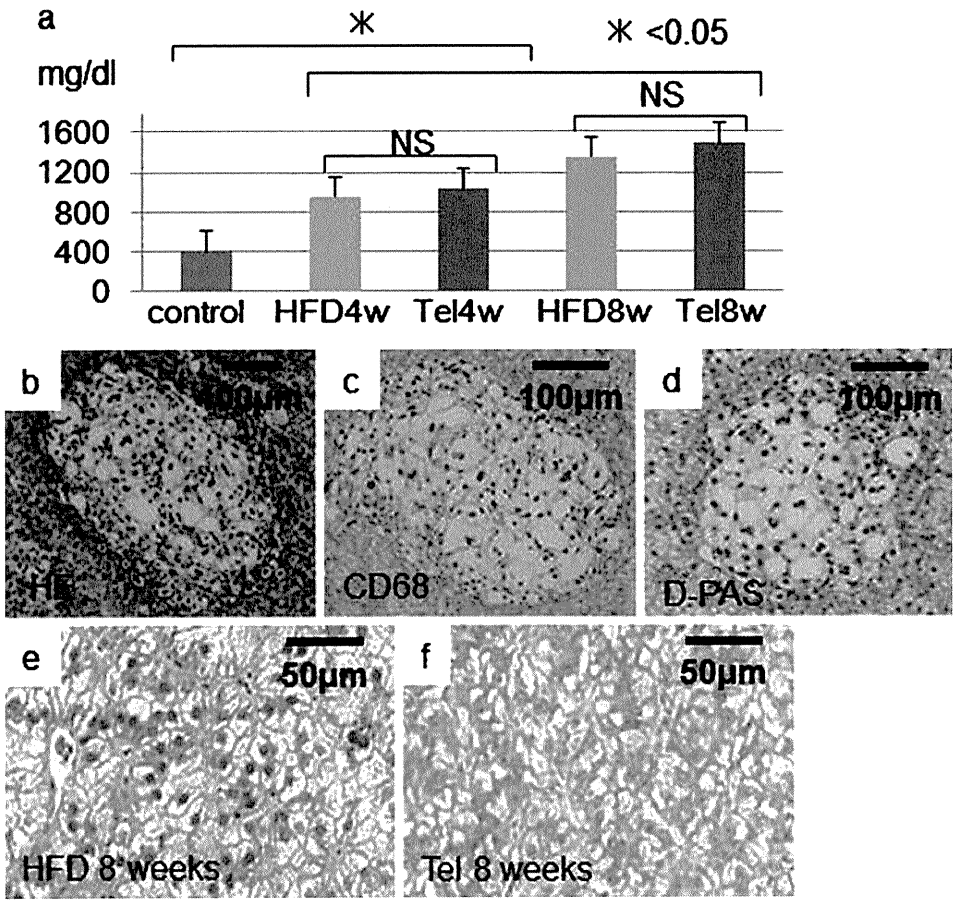

Fig. 5 Blood tests for TG were carried out on the control, HFD and Tel groups at 4 and 8 weeks (**a**). Compared with the control group, TG increased over time in the HFD and Tel groups. The TG level of the Tel group was slightly higher than that of HFD group. We observed tissue with locally aggregated ballooning hepatocyte degeneration in some areas of medaka NASH model liver tissue (**b**). Cells positive for diastase-periodic-acid-Schiff (*D-PAS*) were found at each location (**d**) and cells positive for the macrophage immunostain CD68 were also found (**c**). The HFD group showed many more cells with nuclei positive for 8-hydroxydeoxyguanosine (**e**) compared with the Tel group (**f**)

al. 2004; Weisberg et al. 2006). Moreover, insulin resistance and arteriosclerosis are clearly suppressed in CC chemokine receptor 2 (CCR2)-deficient mice (Ishibashi et al. 2004; Weisberg et al. 2006). Haukeland et al. (2006) report that serum concentrations of monocyte chemotactic protein 1 (MCP1) begin to increase with simple steatosis, peaking with NASH. These findings imply that macrophage infiltration plays an important role in the initiation of metabolic syndrome. MCP1 induces the migration of mononuclear leukocytes by combining with complement receptor type 2 (Fox et al. 1997). A recent study has shown that PPAR-γ agonists inhibit CCR2 expression in mononuclear leukocytes (Tanaka et al. 2005). Tel has also been reported to suppress macrophage infiltration by blocking the MCP1/CCR2 pathway in a mouse NASH model (Kudo et al. 2009). In our medaka NASH model, Tel might suppress macrophage migration to the liver.

In this medaka NASH model, oxidative stress has been evaluated by 8-OHdG immunostaining and has been found to be attenuated by Tel administration (Fig. 5e, f). Hepatocyte apoptosis has been reported as being the key to the second "hit" in the progression from simple steatosis to NASH in human NAFLD and is a significant pathological characteristic of NASH (Feldstein et al. 2003). Hepatocyte apoptosis in liver tissue from the medaka NASH model increases as a result of HFD administration, suggesting that apoptosis is linked to the progression from simple steatosis to NASH and disease development in the medaka NASH model (Fig. 6). One possible underlying mechanism is that the increased apoptosis is related to oxidative stress caused by HFD administration. In the present study, the suppression of apoptosis is greater in the Tel group than in the HFD group.

With regard to liver lipid metabolism, lipid deposited in the fatty liver is in the form of TG. This is attributable to changes in the balance between TG uptake into the liver and secretion out of the liver and to the balance between intrahepatic TG synthesis and breakdown. In our medaka NASH model, the influx of fats into the liver is likely to increase as a result of HFD; greater intrahepatic TG deposition is observed in the HFD group compared with the control group. Whereas no clear difference in FAS is apparent, the reduced expression of ACC1 in the HFD group probably indicates the decrease of de novo fatty acid synthesis pathways even within the relatively short time-scale of 2–4 weeks. With respect to fatty acid oxidation pathways (CPT1 and ACO1), HFD administration appears to increase the oxidation of fatty acids, which is further

Table 4 Fatty acid composition of total lipids in livers of control, HFD medaka and HFD+Tel medaka (1 sample=10 fish; *SFA* saturated fatty acid, *MUFA* mono-unsaturated fatty acid, *PUFA* polyunsaturated fatty acid)

Fatty acid (mol%)	Control	HFD	HFD+Tel
C14 : 0	3.0	16.2	14.3
C16 : 0	48.6	179.4	202.4
C18 : 0	25.8	53.9	55.2
C16 : 1 n-7	3.9	41.7	50.8
C18 : 1 n-9	25.1	514.1	533.9
C20 : 3 n-9	0.7	17.1	16.7
C18 : 2 n-6	11.8	45.0	52.2
C18 : 3 n-6	1.4	28.2	35.3
C20 : 3 n-6	2.3	5.5	3.8
C20 : 4 n-6	11.0	31.9	32.9
C18 : 3 n-3	1.1	1.7	5.2
C20 : 5 n-3	1.8	0.0	1.1
C22 : 6 n-3	62.1	28.8	28.1
Total SFA	78.4	252.5	275.2
Total MUFA	31.3	565.1	591.8
Total PUFA	99.9	164.0	180.5
n-3 PUFA	70.4	32.0	36.1
n-6 PUFA	28.9	114.9	127.7
n-3/n-6 ratio	2.4	0.3	0.3
Total lipid (mg/g tissue)	209.6	981.6	1047.5

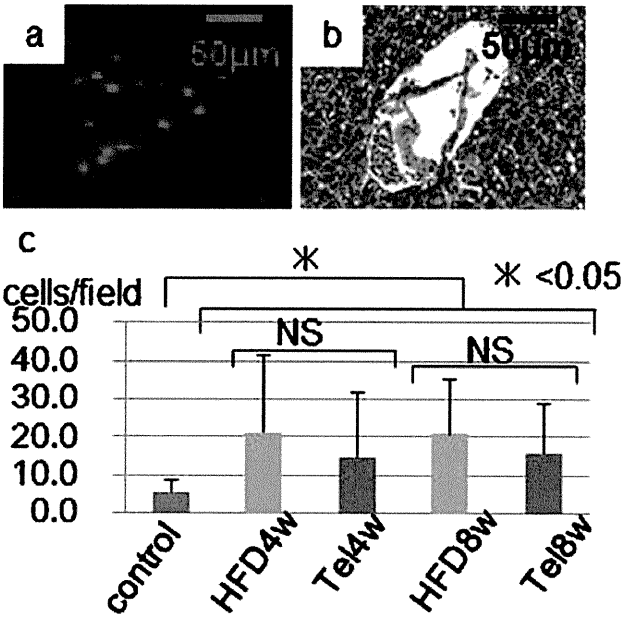

Fig. 6 **a** Investigation of induction of apoptosis-positive cells in liver tissue by TUNEL staining. **b** Same tissue with HE staining. **c** The number of apoptotic cells was greater in the HFD group at 8 weeks than in the control group at 4 weeks (*P<0.05)

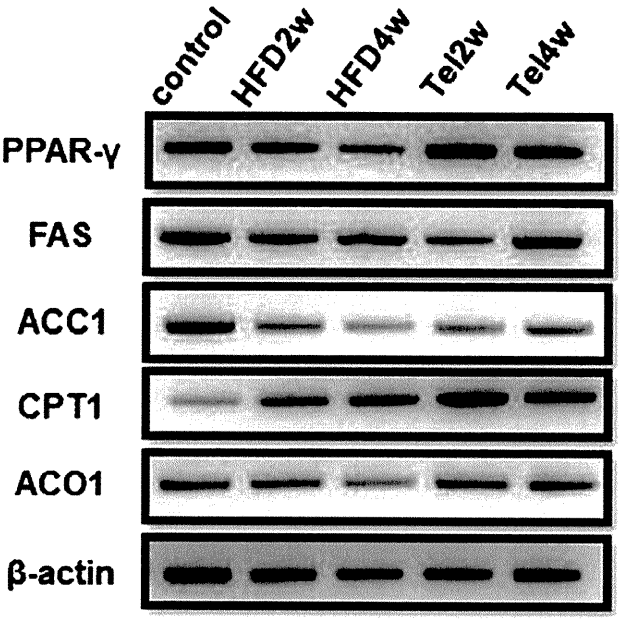

Fig. 7 PPAR-γ expression increased in the Tel group. No clear changes in expression levels of FAS were found in either the HFD or Tel groups compared with the control group. ACC1 mRNA expression in both the HFD and Tel groups was lower than in the control group. CPT1 mRNA expression was higher in the HFD group than in the control group and even higher in the Tel group. ACO1 expression was lower in the HFD group than in the control group. The expression levels of ACO1 were similar in the Tel and control groups (*PPAR-γ* peroxisome proliferator-activated receptor-γ, *FAS* fatty acid synthase, *ACC1* acetyl-CoA carboxylase 1, *CPT1* carnitine palmitoyltransferase 1, *ACO1* acyl CoA oxidase 1)

increased by Tel administration. We have not assessed any direct changes of TG or lipid content of the liver in this series of experiments, despite TG deposition being the primary factor for the formation of fatty liver. However, Tel ameliorates steatosis in the liver. We have also shown that CPT1 and ACO1 expression is increased in the liver on administration of Tel. Thus, the administration of Tel may induce the β-oxidation of free fatty acids in the liver of medaka and thereby also contribute to the reduction of TG in the liver. We consider that this evidence demonstrates the effectiveness of Tel on TG or the oxidation of lipids.

In this study, we have investigated the pharmaceutical effectiveness of Tel, including its potential mechanisms of action. Tel seems to improve NASH, with the inhibition of macrophage infiltration and oxidative stress in the liver, but does not affect the n3/n6 PUFA ratio in NASH liver. These results show that Tel has a different drug effect on NASH and the n3/n6 PUFA ratio. Thus, the medaka NASH model is likely to become a significant experimental model for use in future NAFLD/NASH studies.

In conclusion, we have demonstrated that the medaka model produced on HFD exhibits the same changes as those seen in human NASH pathology. Furthermore, our study confirms that Tel has an effect on this model.